

Perfect Absorption by an Atomically Thin Crystal

Jason Horng^{1,2,*}, Eric W. Martin¹, Yu-Hsun Chou,^{1,3} Emmanuel Courtade,⁴ Tsu-chi Chang,³ Chu-Yuan Hsu,³ Michael-Henr Wentzel¹, Hanna G. Ruth,¹ Tien-chang Lu,³ Steven T. Cundiff,¹ Feng Wang,² and Hui Deng¹

¹ Physics Department, University of Michigan, 450 Church Street, Ann Arbor, Michigan 48109-2122, USA

² Department of Physics, University of California at Berkeley, Berkeley, California 94720, USA

³ Department of Photonics, College of Electrical and Computer Engineering, National Chiao Tung University, Hsinchu 300, Taiwan

⁴ Universite de Toulouse, INSA-CNRS-UPS, LPCNO, 135 Avenue de Rangueil, Toulouse 31077, France

(Received 17 August 2019; revised 30 June 2020; accepted 10 July 2020; published 5 August 2020)

Optical absorption is one of the most fundamental processes in light-matter interactions. The ability to achieve and control high absorption is crucial for a broad range of modern photonic technologies. In nanomaterials of length scales much smaller than a wavelength, optical absorption is typically a weak perturbation. To achieve high absorption, exquisite techniques and structures have been developed, such as coherent interference of multiple laser beams and plasmonic metasurfaces. Here, we show that a robust critical-coupling condition exists to allow perfect absorption of light by a subnanometer-thick two-dimensional semiconductor, when the radiative-decay rate of the exciton resonance balances with its loss rate. We measure an absorption up to 99.6% in a monomolecular MoSe₂ crystal placed in front of a flat mirror. We furthermore demonstrate control of the perfect absorption by tuning the exciton-phonon, exciton-exciton, and exciton-photon interactions with temperature, pulsed laser excitation, and a movable mirror, respectively. Our work suggests a mechanism to achieve and control critical coupling in two-dimensional excitonic systems, enabling photonic applications including ultrafast low-power light modulators and sensitive optical sensing.

DOI: 10.1103/PhysRevApplied.14.024009

I. INTRODUCTION

The achievement of strong absorption of electromagnetic energy by a material is essential for efficient optoelectronics devices. Perfect absorption of light with controllable light-matter interactions has led to the development in photonics for energy harvesting [1,2], sensing [3–5], and modulating and computing applications [6,7]. One typical design to realize destructive interference in all output channels utilizes multiple resonances in lossy metamaterials and plasmonic structures [8–10]; all require precise design and engineering of complex photonic structures. Another approach uses semiconductor layers (Ge, amorphous silicon, and transition-metal dichalcogenide) with highly absorbing band-to-band transitions on metal surfaces to achieve near-unity absorption for ultrathin photodetectors and solar cells [1,11,12]. While both methods lead to strong and broadband absorption features, it is difficult to control the absorption in the fabricated devices consisting of bulk materials.

Among the choices of materials, semiconductors are one of the best optical absorbers due to their well-established optical nonlinearity and electrical controllability. The absorption at the semiconductors' exciton resonances is greatly enhanced and possesses strong nonlinearity due to the coherent nature of the exciton dipole [13,14]. Up to a few percent of absorption can be obtained in a high-quality gallium arsenide (GaAs) quantum well a few nanometers thick [15,16]. Nevertheless, excitonic absorption remains an incoherent and perturbative process in typical low-dimensional semiconductors without using high-quality cavities, multiple coherent laser beams, or precisely engineered metasurfaces and metal interfaces [3,17–20]. In two-dimensional (2D) transition-metal dichalcogenide (TMD) monolayers, the exciton transition dipole moment is almost 2 orders of magnitude stronger than in a GaAs quantum well, resulting from the reduced Coulomb screening in 2D materials [21–23]. High reflectivity has been reported from monolayers at low temperatures [24,25], suggesting that the absorption and remission become coherent in the limit where the radiative decay dominates over pure dephasing and inhomogeneous broadening.

*jahorng@umich.edu

Here, by tuning between the incoherent and coherent limits of exciton absorption in a monolayer placed in front of a mirror, we demonstrate critical coupling between 2D excitons and resonant free-space light, leading to perfect absorption of light in a subnanometer-thick crystal [26]. Up to 99.6% absorption is measured in a MoSe₂ monolayer. Furthermore, we show that the condition for perfect absorption is controlled through the balance between the exciton radiative-decay rate and the scattering rate; therefore, it is readily tuned by temperature tuning of the exciton-phonon scattering, by ultrafast laser control of the exciton-exciton scattering, and by tuning of the exciton-photon interactions with a movable mirror. Our work establishes 2D TMDs as a simple and versatile platform for the engineering of exciton-light interactions and the control of perfect absorption.

II. ANALYSIS OF PERFECT ABSORPTION IN 2D SEMICONDUCTORS

When the light-matter coupling is considered self-consistently, the absorption spectrum of a homogeneous thin-film semiconductor, $\alpha(E)$, for a resonance at energy E_R , is

$$\alpha(E) = \frac{2\Gamma_{\text{sca}}\Gamma_{\text{rad}}}{(E - E_R)^2 + (\Gamma_{\text{sca}} + \Gamma_{\text{rad}})^2}, \quad (1)$$

where Γ_{sca} and Γ_{rad} are the scattering and radiative-decay rates, respectively. This absorption can be understood by a simple microscopic model of exciton absorption, shown in Fig. 1(a). In this model, a resonant plane-wave light field illuminates a homogeneous 2D sheet of dipoles, creating an exciton polarization that either radiatively decays at rate Γ_{rad} or scatters at rate Γ_{sca} . Γ_{rad} is directly proportional to the exciton transition dipole moment. It accounts for the coherent re-emission process that returns energy to the field. Γ_{sca} includes all mechanisms that scatter the excitons to another state, such as exciton-phonon scattering, exciton-impurity scattering, and nonradiative recombination.

In typical semiconductors, because $\Gamma_{\text{sca}} \gg \Gamma_{\text{rad}}$, the energy carried by the optically excited excitons is predominantly transferred into nonradiative-decay channels and Eq. (1) reduces to the Elliott formula for excitonic absorption in the perturbative regime [27]. In this incoherent limit, the total integrated absorption only depends on Γ_{rad} , which is therefore independent of the temperature or the excitation power. The constant integrated absorption, A_0 , is determined by the total number of oscillators in the material, as required by the oscillator sum rule.

However, as the radiative-decay becomes comparable to or larger than scattering or pure dephasing, re-emission of excitons into the optical field is no longer negligible.

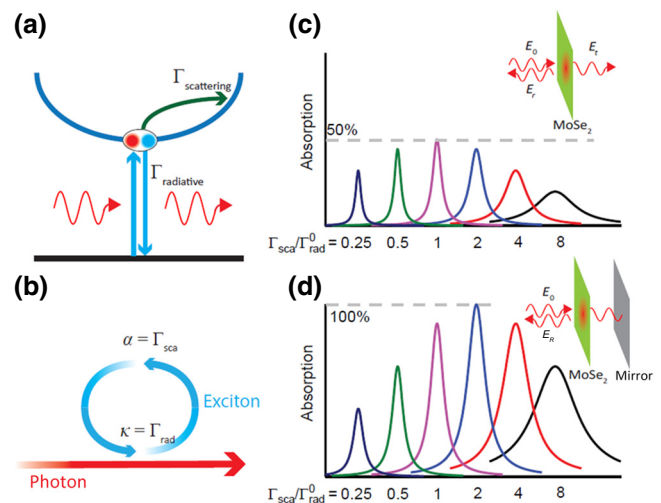


FIG. 1. The absorption mechanism in an excitonic system. (a) The microscopic mechanism of excitonic absorption. After excitation by absorbing a photon, the exciton polarization decays through either radiative recombination or scattering to other states, with rates Γ_{rad} and Γ_{sca} , respectively. Only Γ_{sca} causes energy loss and induces optical absorption. (b),(c) The absorption spectra of a free-standing 2D film (b) and a 2D film in front of a mirror (c), with varying scattering rates. In the free-standing 2D cases, the total absorption decreases as the scattering processes are suppressed. The maximum absorption can reach 50% and 100% in cases (b) and (c), respectively, when the integrated area is decreased to half. (d) An analogy to a ring resonator for the case in (c). The critical-coupling effect between free-space photons and excitons can occur in TMD monolayers. The photon channel is coupled with the exciton channel, with an input coupling efficiency of Γ_{rad} . While the energy is transferred to the exciton channel, scattering processes can create loss with rate Γ_{sca} . The critical-coupling condition is reached if $\Gamma_{\text{sca}} = \Gamma_{\text{rad}}$ and the absorption approaches 100%.

When consistently solved using Eq. (1), the normalized integrated absorption is the ratio of the exciton loss rate in the material and the total rate of exciton decay. The absorption decreases with decreasing Γ_{sca} for fixed Γ_{rad} . At $\Gamma_{\text{sca}} \ll \Gamma_{\text{rad}}$, $\alpha(\omega)$ vanishes and the excited semiconductor reradiates the entire excitation, which yields 100% reflection at the resonance [24,25]. The reduction of the integrated area is, therefore, direct evidence of the excitonic medium reaching the coherent limit and for observing perfect absorption, as explained later.

The transition from the coherent limit ($\Gamma_{\text{sca}} \ll \Gamma_{\text{rad}}$) to the incoherent limit ($\Gamma_{\text{sca}} \gg \Gamma_{\text{rad}}$) is illustrated in Fig. 1(b) for a free-standing excitonic monolayer. In the incoherent limit, the maximum absorption increases with Γ_{sca} and therefore the total line width is decreased to maintain an approximately constant total absorption (the area under the absorption spectrum). In the coherent limit, the maximum absorption decreases while the total line width also

decreases, leading to decreasing total absorption. The maximum linear absorption peaks at 50% when $\Gamma_{\text{sca}} = \Gamma_{\text{rad}}$ due to the mirror symmetry of the monolayer [18].

Perfect absorption, which requires overcoming the 50% maximum absorption, can be achieved by means such as by introducing another laser beam to form a two-port device [6,7,28]. Alternatively, we show that it can also be achieved by breaking the mirror symmetry [3,19], by simply putting a mirror behind the 2D exciton medium [see Fig. 1(d)]. Critical coupling can be established to achieve perfect absorption due to interference between reflection and transmission.

To understand perfect absorption intuitively, we consider the case in which resonant light illuminates a monolayer placed one quarter wavelength away from the mirror. In the incoherent limit, the monolayer has high transmission and most of the incident light is reflected by the mirror, leading to a net reflection coefficient $r = 1$ (referenced to the monolayer). In the coherent limit, the monolayer alone acts as a perfect reflector on resonance, resulting in a reflection coefficient $r = -1$. Since the reflection coefficient at the exciton resonance is real valued, it must go through zero to transition from the incoherent to coherent limit. That is, a critical-coupling condition that gives perfect absorption must exist. As we show below, the perfect absorption condition is robust against inhomogeneous broadening and for arbitrary monolayer-to-mirror distances, since it is required by the continuity of the reflection coefficient.

Quantitatively, the reflection coefficient can be obtained by considering all multiple reflections. The reflection and transmission coefficients of a free-standing monolayer in the linear regime are $r_m(E) = i\Gamma_{\text{rad}}^0/[E - E_R - i(\Gamma_{\text{sca}} + \Gamma_{\text{rad}}^0)]$ and $t_m(\omega) = 1 + r_m(\omega)$. The total reflection coefficient $r(E)$ can be calculated by considering all multiple reflections leading to $r = ([\exp(i\phi) + 2]r_m + 1)[\exp(i\phi) - r_m]$, where ϕ is the phase accumulation during the traveling between the monolayer and the mirror. When the monolayer is placed at $\lambda/4$ away from the mirror, $\phi = 2\pi$ and $r = (3r_m + 1)/(1 - r_m)$. The critical-coupling condition occurs when $\Gamma_{\text{sca}} = \Gamma_{\text{rad}} = 2\Gamma_{\text{rad}}^0$, $r_m(E_R) = -1/3$ leading to $r = 0$ and perfect absorption. To see the robustness of the critical-coupling condition, we look for the zeros of the reflection coefficient while analytically continuing E to the complex plane. This leads to

$$E_{\text{zero}} = E_R + i \left(\Gamma_{\text{sca}} - \frac{\exp(i\phi) + 1}{2} 2\Gamma_{\text{rad}} \right). \quad (2)$$

Assume that we have a tuning parameter s to tune $E_R(s)$, $\Gamma_{\text{sca}}(s)$, and $\Gamma_{\text{rad}}(s)$. In the incoherent limit, $\Gamma_{\text{sca}} \gg \Gamma_{\text{rad}}$; therefore the solution E_{zero} lies in the upper plane, which is an unphysical solution. In the coherent limit, $\Gamma_{\text{sca}} \ll \Gamma_{\text{rad}}$,

E_0 lies in the lower plane for all ϕ values except π . Since the solution E_{zero} must move continuously when we tune the system from the incoherent to the coherent limit, it unavoidably crosses the $\text{Re}(E)$ axis, leading to a physical solution, corresponding to perfect absorption. Note that as long as the E_0 moves across two sides of the $\text{Re}(E)$ axis for two limits, this argument holds even when inhomogeneous broadening is introduced.

Critical coupling can also be understood as an analogy to a ring resonator, as illustrated in Fig. 1(d). The photon channel corresponds to the linear waveguide and the exciton channel corresponds to the ring waveguide. Γ_{rad} and Γ_{sca} correspond to the input coupling efficiency and the loss in the ring waveguide, respectively. Similar to the ring resonator, $\Gamma_{\text{sca}} = \Gamma_{\text{rad}}$ corresponds to a critical-coupling condition where all the energy is trapped in the exciton channel and does not re-emit into photons.

III. EXPERIMENTAL IMPLEMENTATION

To achieve perfect absorption, the coherent limit of exciton absorption must be demonstrated and a knob to tune the system between the two limits is needed. We use a high-quality hexagonal-boron-nitride (*h*-BN) encapsulated MoSe₂ monolayer placed on a distributed Bragg reflector (DBR) with high reflectance. The reported exciton binding energy in encapsulated MoSe₂ monolayers is around 200 meV [29], exhibiting a strong excitonic feature even at room temperature. The sample is prepared by mechanical exfoliation of bulk MoSe₂ (from 2D Semiconductors, USA) and *h*-BN crystals [30]. Using the all-dry viscoelastic stamping technique [31], MoSe₂ monolayers are first identified by optical contrast on polydimethylsiloxane (PDMS) and then transferred onto a DBR and a sapphire substrate (for the distance-dependent measurement) to obtain the *h*-BN/MoSe₂ monolayer/*h*-BN stacking. After the sample is made, we measure the strong photoluminescence from the sample to double confirm that it is a monolayer MoSe₂ with a direct band gap. The thickness of the *h*-BN is determined through atomic force microscopy after the transfer process. The home-made DBR mirror is made of 12 pairs of electron-beam-evaporated SiO₂ and TiO₂ layers on top of a sapphire substrate. We measure $99.8 \pm 0.02\%$ reflectivity in the stop band ranging from 690 to 800 nm, with a small temperature dependence (for measured reflection spectra of the DBR, see Fig. S1 in the Supplemental Material [32]). In the final sample, we have a structure of vacuum / 9-nm *h*-BN/1-nm MoSe₂/12.5-nm *h*-BN/129-nm SiO₂/79-nm TiO₂ / ... / 129-nm SiO₂ / 79-nm TiO₂. Ideally, we want the monolayer positioned close to the field maximum, to enhance the radiative-decay rate and bring the system closer to the coherent limit. A transfer-matrix method is used to simulate the electromagnetic

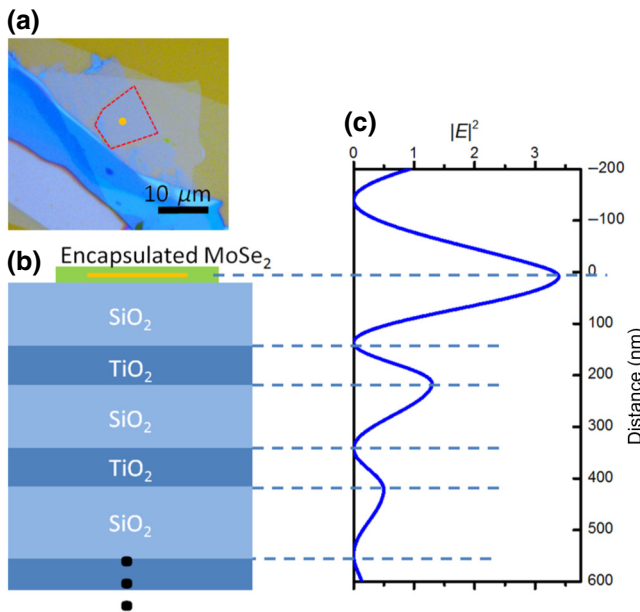


FIG. 2. The sample structure and local field enhancement from a distributed Bragg reflector (DBR). (a) An optical-microscope image of the sample. The red lines encircle the MoSe_2 monolayer area. The orange dot labels the location of the measurements. (b) A schematic of the sample structure. The sample is designed such that the MoSe_2 monolayer is $\lambda/4$ away from the DBR mirror to ensure the largest absorption and radiative enhancement. (c) A simulation of the position-dependent squared electric field for photon energy 1.650 eV, showing that the MoSe_2 monolayer is close to the antinode of the standing light wave.

wave propagation in our multilayer sample structure [Fig. 2(c)].

To take reflection spectroscopy, the encapsulated MoSe_2 on DBR sample is mounted in a cryostat (Montana Instruments) with closed-loop temperature control. A broadband tungsten lamp or a femtosecond Ti:sapphire laser with 20-nm bandwidth (for laser power dependence) is focused onto the sample via a $50\times$ long-working-distance objective lens with a 0.42 numerical aperture. The reflected light is selected by a confocal aperture equivalent to a spot size $2 \mu\text{m}$ in diameter. The light is collected into a grating spectrometer (Princeton Instruments) with a spectral resolution of 0.2 nm, together with a charge-coupled device for recording the light intensity. The temperature-dependent spectra are taken in the 10–300 K range and the power-dependent spectra are taken at 5 K. The absorption spectrum, $\alpha(E)$, is obtained directly from $\alpha(E) = 1 - R_m(E)/R_s(E)$, where R_m and R_s are the measured reflection spectra from the location with and without the monolayer, respectively. Figures 2(a) and 2(b) show an optical image of the sample studied and a schematic of the overall structure. All data (except for the distance-dependent spectra) are taken at the orange spot but other areas show similar behavior.

IV. CONTROL OF PERFECT ABSORPTION

To tune the system between the incoherent and coherent regimes, we first use temperature tuning to control the ratio $\Gamma_{\text{sca}}:\Gamma_{\text{rad}}$, because the contribution of phonon scattering to Γ_{sca} should decrease with decreasing temperature, while Γ_{rad} is largely independent of temperature due to the large exciton binding energy [33,34]. The justification of constancy of Γ_{rad} over the temperature range is shown below. The radiative line width is directly related to the oscillator strength f of the exciton by the following formula: $\Gamma_{\text{rad}} = (2\pi/n)(e^2/m_0c)(f/S)$ [Eq. (51) in Ref. [34]], where n is the refractive index, m_0 the electron mass, and S is the area. Microscopically, $f = g(2|\epsilon \cdot p_{cv}|^2/m_0\hbar\omega)V(1/\pi a_B^3)$ [Eq. (15) in Ref. [34]], where g is the degeneracy, p_{cv} is the interband-momentum matrix element, V is the volume, and a_B is the Bohr radius. p_{cv} and a_B are modified only slightly by the elevated temperature (up to room temperature), since the binding energy of 200 meV is significantly higher than the energy corresponding to room temperature. Therefore, the oscillator strength of the A exciton is mostly constant over the temperature range, as required by the optical-sum rule. This has been checked theoretically by Brem *et al.* [33] and experimentally by Scuri *et al.* [25].

Figure 3(a) shows the temperature dependence of the reflection spectra near the A -exciton resonance. The B exciton is 200 meV above the A exciton and is not relevant to the current discussion. At 270 K, the A -exciton absorption at 1.59 eV has 32% contrast and a line width of approximately 40 meV. With decreasing temperature, the line width of the exciton absorption narrows nearly 7-fold, from 40 meV to 6.1 meV [Fig. 3(c)]. As shown in Fig. 3(b), the temperature evolution of the exciton energies can be fitted well by the Varshni formula, $E_g = E_0 - \alpha T^2/(T + \beta)$, which describes the band-gap increase with decreasing temperature [35]. Fitting yields $E_0 = 1.653$ eV, $\alpha = 0.48$ meV/K, and $\beta = 211$ K, in good agreement with previously reported results [22].

The exciton resonance also shifts with temperature, which could affect the enhancement of the radiative-decay rate due to the local field factor from the mirror. To quantify the effect, we apply a transfer-matrix calculation to estimate the local field factor for the photon energy. Corresponding to the energy shift from 1.593 to 1.653 eV, we estimate that the local field factor $|E_{\text{local}}|^2$ changes by 14% [orange in Fig. 3(b)]. This is a small change compared to the change of the total line width, indicating that the change in the integrated absorption is mainly caused by line-width narrowing. The main uncertainty of the calculation comes from the uncertainty of the refractive indices ($n_{\text{h-BN}} = 1.8\text{--}2.0$, $n_{\text{SiO}_2} = 1.45\text{--}1.5$, $n_{\text{TiO}_2} = 2.35\text{--}2.5$) in the calculation and the plot the result in the error bars of Fig. 3(b).

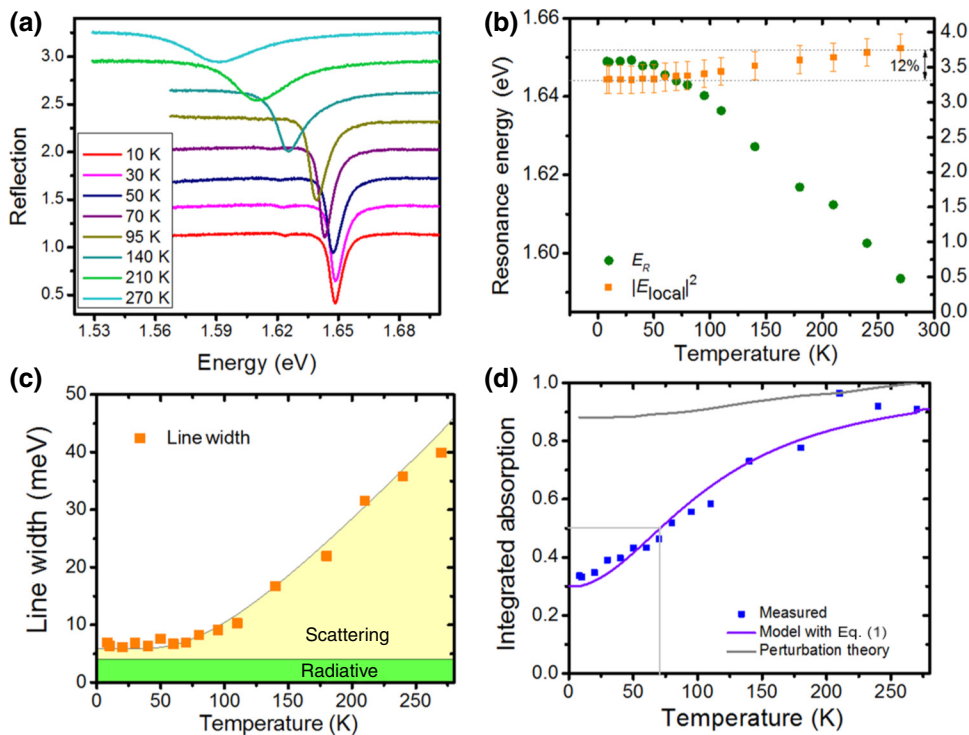


FIG. 3. The reduced optical absorption in the coherent limit. (a) Measured reflection spectra near the A -exciton resonance of the MoSe_2 monolayer at different temperatures. The spectra are offset for clarity. (b) The temperature-dependent exciton resonance energy is shown in olive squares. The simulated $|E_{\text{local}}|^2$ at the MoSe_2 position for the corresponding exciton wavelength at each temperature is plotted in orange squares. The absorption enhancement factor varies within 14% over the whole temperature range. The error bar originates from the uncertainty of the refractive indices. (c) Measured exciton line widths versus the temperature. The shaded areas show line-width contributions from radiative (green) and scattering (yellow) broadenings. (d) The measured (blue squares) and fitted (violet curve) integrated absorption as a function of the temperature. The gray line shows the prediction from the perturbative theory, taking into account the wavelength-dependent absorption enhancement. A remarkable 67% reduction in integrated absorption is observed experimentally, indicating that coherent absorption dominates.

The temperature dependence of the normalized integrated absorption A/A_0 is shown in Fig. 3(d). The gray curve shows the prediction from the perturbative theory, where a linear relationship between the absorption and the susceptibility is assumed, after accounting for the 14% change due to the shift of the exciton resonance. Clearly, the measured integrated absorption does not agree with the perturbative theory, showing instead the transition from the incoherent to the coherent limit as A/A_0 decreases from near unity to a mere 33%. The large reduction of the integrated absorption upon cooling shows that the exciton-phonon scattering dominates at high temperatures but it is greatly suppressed at low temperatures [36]. As Γ_{sca} is reduced, the system approaches the coherent limit.

The measured temperature dependence of integrated absorption can be compared with the nonperturbative theory. From Eq. (1), we obtain the integrated absorption as $A/A_0 = \Gamma_{\text{sca}}/(\Gamma_{\text{sca}} + \Gamma_{\text{rad}})$. Here, we apply this equation and use the temperature-independent $\hbar\Gamma_{\text{rad}}$ and A_0 as free parameters to find the best fit for the measured line width $\hbar\Gamma_{\text{tot}}$ and the integrated absorption A , simultaneously. The

fitting results are shown in Fig. 3(c) (gray curve) and Fig. 3(d) (purple curve), showing nice agreement with the experimental data. The fit yields $\hbar\Gamma_{\text{rad}} = 4.0 \pm 0.2$ meV and $A_0 = 19.3 \pm 0.5$ meV. The radiative line width can also be checked independently, as it is directly proportional to the measured integrated absorption at high temperatures, where $\Gamma_{\text{sca}} \gg \Gamma_{\text{rad}}$ and $A \approx A_0$. From the transfer-matrix simulation, the A_0 value corresponds to $\hbar\Gamma_{\text{rad}} = 3.9 \pm 0.2$ meV, in excellent agreement with the fitted $\hbar\Gamma_{\text{rad}}$. The minimal normalized integrated absorption A/A_0 is measured to be 33% at 10 K, which corresponds to a finite $\hbar\Gamma_{\text{sca}} = 2.1$ meV resulting from inhomogeneity and exciton-impurity scattering. It can be further reduced by improving the sample quality [37,38]. Nonetheless, the absorption decreases to below $A_0/2$ and should reach the critical-coupling condition at $\Gamma_{\text{sca}} = \Gamma_{\text{rad}}$.

Figure 4(a) shows absorption spectra versus the temperature from 110 K to 10 K. With decreasing temperature, the maximum absorption at the exciton resonance first increases, as expected from the reduction in line width at low temperature, but then decreases from 70 K to

10 K. A maximal absorption of 94.6% is achieved at $T_c = 70$ K, showing critical coupling between the photons and excitons. The critical temperature of $T = 70$ K corresponds to the point at which $\Gamma_{\text{sca}} = \Gamma_{\text{rad}}$ and the integrated absorption $A/A_0 = 50\%$, as shown in Figs. 3(c) and 3(d), respectively. Thus we demonstrate critical coupling between excitons and free-space photons in a monolayer TMD.

Besides temperature tuning of Γ_{sca} via the phonon-exciton scattering, the strong nonlinear exciton-exciton scattering in TMDs enables the tuning of Γ_{sca} using an ultrafast pulsed laser. The pulsed laser has enough spectral bandwidth to cover the exciton peak for reflection measurements. As shown in Fig. 4(b), with increasing excitation power, the absorption peak first increases in height and then decreases, with a nearly perfect absorption of 99.6% where the critical-coupling condition is met. At the same time, the line width of the absorption peak increases monotonically with increasing excitation power, consistent with the change in absorption resulting from changing Γ_{sca} . Solving Eq. (1) and maintaining the condition that $\Gamma_{\text{tot}} = \Gamma_{\text{sca}} + \Gamma_{\text{rad}}$, we obtain Γ_{sca} and Γ_{rad} , as shown in the upper panel of Fig. 4(b). As the excitation power increases by a factor of 10, the radiative line width remains constant while the scattering rate Γ_{sca} quickly increases from 2 meV to 9 meV, quadratically with the power, as expected for exciton-exciton scattering. Reflection spectra for both increasing and decreasing laser-power sweeps are measured (shown in Fig. S2 in the Supplemental Material [32]) to eliminate the heating effect and the sample-damaging effect. The increasing laser-power trend and the reducing power trend are identical. The repeatability excludes the heating effect and the sample-damaging effect. Our results demonstrate tuning of the absorption up to nearly 100% with a pulsed laser. This effect can be utilized for ultrafast light modulators and can be extended to room temperature by increasing Γ_{rad} via nanophotonic structures [2,39].

Lastly, we demonstrate critical coupling by tuning Γ_{rad} with a movable mirror, as shown in the inset of Fig. 4(c). We prepare another encapsulated MoSe₂ flake on a sapphire substrate and mount the DBR on a piezoelectric stage to vary the vacuum gap distance. The sapphire substrate is clamped on a copper plate with a through hole, while a 2 × 2-mm DBR is mounted on a piezoelectric stage. The parallelism of the DBR and the sapphire substrate is aligned by observing the reflected light in the far field and we ensure that the tilt angle is less than 0.02° throughout the measurements. Before the optical measurements, the DBR is stepped close to the sapphire substrate with a small gap of around 1 μm. During the measurements, we step the piezoelectric stage to tune the monolayer-to-mirror distance and measure reflectance spectra at the same various mirror positions. To calibrate the mirror distance, we utilize the interference pattern due to the DBR and the sapphire substrate over a broad spectral range when they are

sufficiently far apart. The calibration detail is described in Ref. [40]. This measurement is done in a cryostat with the sample temperature at 50 K.

The tuning of the spacing between the sample and mirror modifies the local photon density of states and in turn the radiative-decay rate Γ_{rad} , while the scattering line width is unaffected. The absorption spectra at different mirror distances are shown in Fig. 4(c). The spectra show a strong modulation of the absorption depth. The critical-coupling condition is achieved when the monolayer is positioned at the antinode ($d = 1050$ nm) of the light, with a maximal absorption of 98.9%. The Γ_{sca} and Γ_{rad} values obtained are shown in the upper panel of Fig. 4(c) (for the distance-dependence spectra of another encapsulated WSe₂ sample, see Fig. S3 in the Supplemental Material [32]). The distance-dependence spectra also show close-to-unity absorption, showing the robustness of the critical-coupling condition. Such strong modulation of the radiative line width simply using a mirror results from the large oscillator strength and the 2D nature of monolayer TMDs. Consequently, critical coupling can be reached even with a low radiative enhancement factor.

V. DISCUSSION AND OUTLOOK

In conclusion, we demonstrate a mechanism to achieve and control perfect absorption in MoSe₂ monolayer crystals by tuning the exciton-photon interaction and exciton dynamics. Analogous to critical coupling in ring resonators, as the scattering and radiative rates of the exciton are equal, we show perfect absorption (up to 99.6%) in a subnanometer-thick monolayer in front of a mirror. The perfect absorption takes place as the exciton-photon interaction transitions from the incoherent to the coherent regime, where a nonperturbative treatment of absorption is needed, as evidenced by a significant reduction in the total exciton absorption. The critical-coupling condition for perfect absorption is achieved by tuning the temperature, pulsed laser excitation, and a movable mirror, which tunes the exciton-phonon, exciton-exciton, and exciton-photon coupling, respectively. These results show that TMD monolayers are highly experimentally accessible systems for rich excitonic phenomena resulting from coherent exciton-photon interaction.

Perfect absorption has broad applications, such as ultrafast light modulation [41], optical sensing [3,4,42], coherent optical computing [6,7,43], designs of imaging [44], laser pulse shaping [45], and high-efficiency photodetection for quantum information processing [2,19,46,47]. Our work shows that 2D materials are advantageous compared to previous systems used for perfect absorption because of the feasibility of achieving near-100% absorption, the simplicity of both the configuration and the analytical critical-coupling condition, and the flexibility to control the perfect

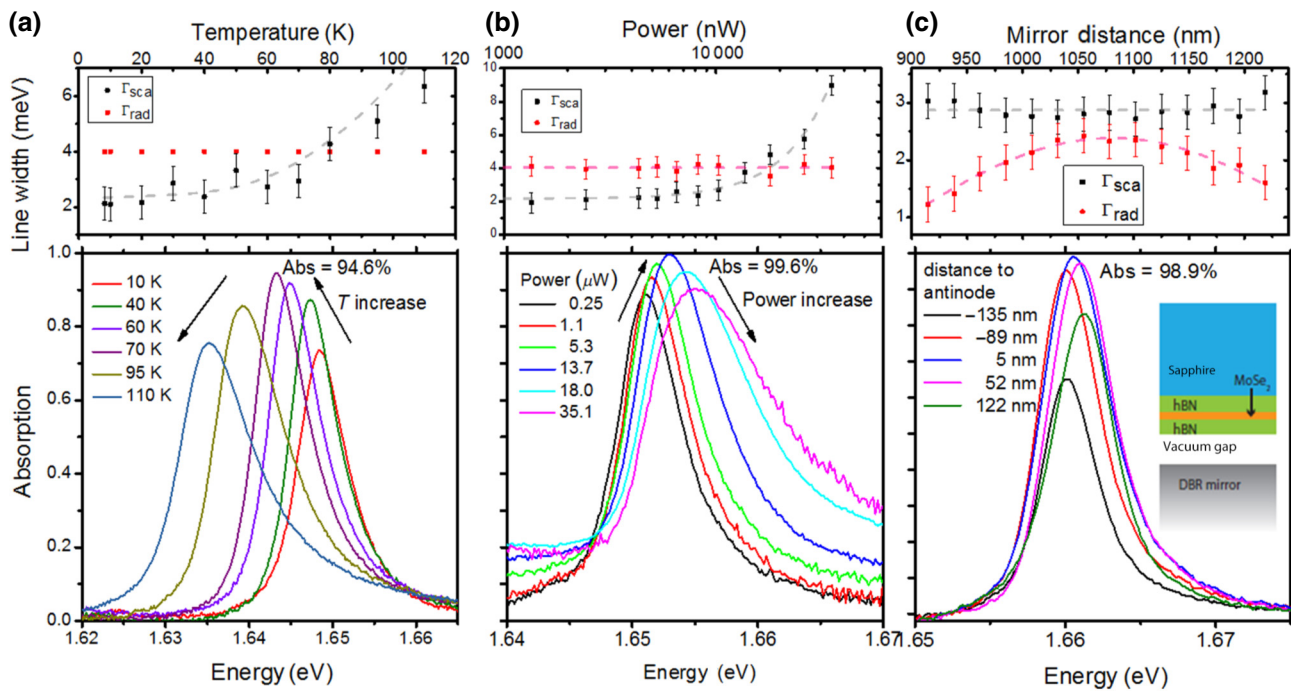


FIG. 4. Observation of the critical-coupling phenomenon between an exciton and a free-space photon. (a)–(c) Measured absorption spectra (lower panels) with the temperature (a), laser intensity (b), and mirror distance (c) as tuning parameters. All three methods show a clear critical-coupling effect with nearly 100% maximum absorption of 94.6%, 99.6%, and 98.9%, respectively. The extracted $\hbar\Gamma_{\text{rad}}$ and $\hbar\Gamma_{\text{sca}}$ are plotted in the corresponding upper panels. The critical-coupling condition occurs when the temperature, laser intensity, and mirror distance are tuned such that $\Gamma_{\text{rad}} = \Gamma_{\text{sca}}$.

absorption condition via a variety of methods. In particular, controlling the critical-coupling condition via ultrafast pulsed excitation may allow ultrafast switching or modulation that is difficult to implement in other systems. The strong absorption modulation as a function of the mirror distance suggests, on one hand, that microelectromechanical devices can be used to control the critical-coupling condition with a potentially very low energy cost [48] and, on the other, that such systems may allow the study of vacuum nonlinear back action to the TMD film through the Casimir-Polder effect. More generally, the work provides an example how unconventional coherent phenomena and potential photonic-device applications may result from the two pronounced and advantageous properties of semiconductor 2D materials—the two-dimensionality and the exceptionally high ratio of radiative decay versus the scattering rate.

ACKNOWLEDGMENTS

We gratefully thank Professor Mack Kira and Professor Bernhard Urbaszek for fruitful discussions. J.H. and H.D. acknowledge the support by the Army Research Office (ARO) under Grant No. W911NF-17-1-0312 (MURI: Room Temperature 2D Polaritronics with van der Waals Heterostructures). Y.-H.C. acknowledges the support by the Ministry of Science and Technology in Taiwan for

the Postdoctoral Research Abroad Program and Grant No. 106-2917-I-564-021. E.C. acknowledges a Labex NEXT travel grant.

- [1] Mikhail A. Kats, Romain Blanchard, Patrice Genevet, and Federico Capasso, Nanometre optical coatings based on strong interference effects in highly absorbing media, *Nat. Mater.* **12**, 20 (2013).
- [2] Giuseppe Pirruccio, Luis Martin Moreno, Gabriel Lozano, and Jaime Gómez Rivas, Coherent and broadband enhanced optical absorption in graphene, *ACS Nano* **7**, 4810 (2013).
- [3] Na Liu, Martin Mesch, Thomas Weiss, Mario Hentschel, and Harald Giessen, Infrared perfect absorber and its application as plasmonic sensor, *Nano Lett.* **10**, 2342 (2010).
- [4] Jason Horng, Halleh B. Balch, Allister F. McGuire, Hsin-Zon Tsai, Patrick R. Forrester, Michael F. Crommie, Bianxiao Cui, and Feng Wang, Imaging electric field dynamics with graphene optoelectronics, *Nat. Commun.* **7**, 13704 (2016).
- [5] Azadeh Kiani Sarkaleh, Babak Vosoughi Lahijani, Hamidreza Saberkari, and Ali Esmaeeli, Optical ring resonators: A platform for biological sensing applications, *J. Med. Signals Sens.* **7**, 185 (2017), publisher: Medknow Publications & Media Pvt Ltd.
- [6] Jianfa Zhang, Kevin F. MacDonald, and Nikolay I. Zheludev, Controlling light-with-light without nonlinearity, *Light: Sci. Appl.* **1**, e18 (2012).

- [7] Xu Fang, Kevin F. MacDonald, and Nikolay I. Zheludev, Controlling light with light using coherent metadevices: All-optical transistor, summator and invertor, *Light: Sci. Appl.* **4**, e292 (2015).
- [8] Xianliang Liu, Tatiana Starr, Anthony F. Starr, and Willie J. Padilla, Infrared Spatial and Frequency Selective Metamaterial with Near-Unity Absorbance, *Phys. Rev. Lett.* **104**, 207403 (2010), publisher: American Physical Society.
- [9] Jiaming Hao, Jing Wang, Xianliang Liu, Willie J. Padilla, Lei Zhou, and Min Qiu, High performance optical absorber based on a plasmonic metamaterial, *Appl. Phys. Lett.* **96**, 251104 (2010).
- [10] Y. Ra'di, C. R. Simovski, and S. A. Tretyakov, Thin Perfect Absorbers for Electromagnetic Waves: Theory, Design, Realizations, *Phys. Rev. Appl.* **3**, 037001 (2015), publisher: American Physical Society.
- [11] Junghyun Park, Ju-Hyung Kang, Alok P. Vasudev, David T. Schoen, Hwi Kim, Erez Hasman, and Mark L. Brongersma, Omnidirectional near-unity absorption in an ultrathin planar semiconductor layer on a metal substrate, *ACS Photonics* **1**, 812 (2014).
- [12] Deep Jariwala, Artur R. Davoyan, Giulia Tagliabue, Michelle C. Sherrott, Joeson Wong, and Harry A. Atwater, Near-unity absorption in van der Waals semiconductors for ultrathin optoelectronics, *Nano Lett.* **16**, 5482 (2016).
- [13] Gunnar Björk, Stanley Pau, Joseph Jacobson, and Yoshihisa Yamamoto, Wannier exciton superradiance in a quantum-well microcavity, *Phys. Rev. B* **50**, 17336 (1994).
- [14] Eiichi Hanamura, Rapid radiative decay and enhanced optical nonlinearity of excitons in a quantum well, *Phys. Rev. B* **38**, 1228 (1988).
- [15] M. V. Marquezini, J. Tignon, T. Hasche, and D. S. Chemla, Refractive index and absorption of GaAs quantum wells across excitonic resonances, *Appl. Phys. Lett.* **73**, 2313 (1998).
- [16] R. J. Nelson, N. Holonyak, and W. O. Groves, Free-exciton transitions in the optical absorption spectra of $\text{GaAs}_{1-x}\text{P}_x$, *Phys. Rev. B* **13**, 5415 (1976).
- [17] Y. D. Chong, Li Ge, Hui Cao, and A. D. Stone, Coherent Perfect Absorbers: Time-Reversed Lasers, *Phys. Rev. Lett.* **105**, 053901 (2010).
- [18] Denis G. Baranov, Alex Krasnok, Timur Shegai, Andrea Alù, and Yidong Chong, Coherent perfect absorbers: Linear control of light with light, *Nat. Rev. Mater.* **2**, 17064 (2017).
- [19] Sukosin Thongrattanasiri, Frank H. L. Koppens, and F. Javier García de Abajo, Complete Optical Absorption in Periodically Patterned Graphene, *Phys. Rev. Lett.* **108**, 047401 (2012).
- [20] Wenjie Wan, Yidong Chong, Li Ge, Heeso Noh, A. Douglas Stone, and Hui Cao, Time-reversed lasing and interferometric control of absorption, *Science* **331**, 889 (2011).
- [21] Kin Fai Mak, Changgu Lee, James Hone, Jie Shan, and Tony F. Heinz, Atomically Thin MoS₂: A New Direct-Gap Semiconductor, *Phys. Rev. Lett.* **105**, 136805 (2010).
- [22] Malte Selig, Gunnar Berghäuser, Archana Raja, Philipp Nagler, Christian Schüller, Tony F. Heinz, Tobias Korn, Alexey Chernikov, Ermin Malic, and Andreas Knorr, Exciton linewidth and coherence lifetime in monolayer transition metal dichalcogenides, *Nat. Commun.* **7**, 13279 (2016).
- [23] Maurizia Palummo, Marco Bernardi, and Jeffrey C. Grossman, Exciton radiative lifetimes in two-dimensional transition metal dichalcogenides, *Nano Lett.* **15**, 2794 (2015).
- [24] Patrick Back, Sina Zeytinoglu, Aroosa Ijaz, Martin Kroener, and Atac Imamoğlu, Realization of an Electrically Tunable Narrow-Bandwidth Atomically Thin Mirror Using Monolayer MoSe₂, *Phys. Rev. Lett.* **120**, 037401 (2018).
- [25] Giovanni Scuri, You Zhou, Alexander A. High, Dominik S. Wild, Chi Shu, Kristiaan De Greve, Luis A. Jauregui, Takashi Taniguchi, Kenji Watanabe, Philip Kim, Mikhail D. Lukin, and Hongkun Park, Large Excitonic Reflectivity of Monolayer MoSe₂ Encapsulated in Hexagonal Boron Nitride, *Phys. Rev. Lett.* **120**, 037402 (2018).
- [26] Yilei Li and Tony F. Heinz, Two-dimensional models for the optical response of thin films, *2D Mater.* **5**, 025021 (2018).
- [27] M. Kira and Stephan W. Koch, *Semiconductor Quantum Optics* (Cambridge University Press, Cambridge, 2011).
- [28] Lorenzo Baldacci, Simone Zanotto, and Alessandro Tredicucci, Coherent perfect absorption in photonic structures, *Rendiconti Lincei* **26**, 219 (2015).
- [29] M. Goryca, J. Li, A. V. Stier, T. Taniguchi, K. Watanabe, E. Courtade, S. Shree, C. Robert, B. Urbaszek, X. Marie, and S. A. Crooker, Revealing exciton masses and dielectric properties of monolayer semiconductors with high magnetic fields, *Nat. Commun.* **10**, 4172 (2019).
- [30] T. Taniguchi and K. Watanabe, Synthesis of high-purity boron nitride single crystals under high pressure by using Ba-BN solvent, *J. Cryst. Growth* **303**, 525 (2007).
- [31] Andres Castellanos-Gomez, Michele Buscema, Rianda Molenaar, Vibhor Singh, Laurens Janssen, Herre S. J. van der Zant, and Gary A. Steele, Deterministic transfer of two-dimensional materials by all-dry viscoelastic stamping, *2D Mater.* **1**, 011002 (2014).
- [32] See the Supplemental Material at <http://link.aps.org/supplemental/10.1103/PhysRevApplied.14.024009>, which includes complementary experiments and figures.
- [33] Samuel Brem, Jonas Zipfel, Malte Selig, Archana Raja, Lutz Waldecker, Jonas D. Ziegler, Takashi Taniguchi, Kenji Watanabe, Alexey Chernikov, and Ermin Malic, Intrinsic lifetime of higher excitonic states in tungsten diselenide monolayers, *Nanoscale* **11**, 12381 (2019).
- [34] Lucio Claudio Andreani, in *Strong Light-Matter Coupling* (World Scientific, Singapore, 2013), p. 37.
- [35] Y. P. Varshni, Temperature dependence of the energy gap in semiconductors, *Physica* **34**, 149 (1967).
- [36] S. Shree, M. Semina, C. Robert, B. Han, T. Amand, A. Balocchi, M. Manca, E. Courtade, X. Marie, T. Taniguchi, K. Watanabe, M. M. Glazov, and B. Urbaszek, Observation of exciton-phonon coupling in MoSe₂ monolayers, *Phys. Rev. B* **98**, 035302 (2018).
- [37] You Zhou, Giovanni Scuri, Jiho Sung, Ryan J. Gelly, Dominik S. Wild, Kristiaan De Greve, Andrew Y. Joe, Takashi Taniguchi, Kenji Watanabe, Philip Kim, Mikhail D. Lukin, and Hongkun Park, Controlling excitons in an atomically thin membrane with a mirror, arXiv:1901.08500 (2019).
- [38] Christopher Rogers, Dodd Gray, Jr., Nathan Bogdanowicz, Takashi Taniguchi, Kenji Watanabe, and Hideo

- Mabuchi, Coherent Control of Two-Dimensional Excitons, arXiv:1902.05036 (2019).
- [39] Deniz Umut Yildirim, Amir Ghobadi, and Ekmel Ozbay, Near-absolute polarization insensitivity in graphene based ultra-narrowband perfect visible light absorber, *Sci. Rep.* **8**, 15210 (2018).
- [40] Jason Horng, Yu-Hsun Chou, Tsu-Chi Chang, Chu-Yuan Hsu, Tien-Chang Lu, and Hui Deng, Engineering radiative coupling of excitons in 2D semiconductors, *Optica* **6**, 1443 (2019).
- [41] Xinglin Wen, Zibo Gong, and Dehai Li, Nonlinear optics of two-dimensional transition metal dichalcogenides, *InfoMat* **1**, 317 (2019).
- [42] Xiong Feng, Jinglan Zou, Wei Xu, Zhihong Zhu, Xiaodong Yuan, Jianfa Zhang, and Shiqiao Qin, Coherent perfect absorption and asymmetric interferometric light-light control in graphene with resonant dielectric nanostructures, *Opt. Express* **26**, 29183 (2018).
- [43] A. Goodarzi and M. Ghanaatshoar, Coherent all-optical transistor based on frustrated total internal reflection, *Sci. Rep.* **8**, 5069 (2018).
- [44] Maria Papaioannou, Eric Plum, Edward T. F. Rogers, and Nikolay I. Zheludev, All-optical dynamic focusing of light via coherent absorption in a plasmonic metasurface, *Light: Sci. Appl.* **7**, 17157 (2018).
- [45] Venkatram Nalla, João Valente, Handong Sun, and Nikolay I. Zheludev, 11-fs dark pulses generated via coherent absorption in plasmonic metamaterial, *Opt. Express* **25**, 22620 (2017).
- [46] A. Ü. C. Hardal and Martijn Wubs, Quantum coherent absorption of squeezed light, *Optica* **6**, 181 (2019).
- [47] M. D. Eisaman, J. Fan, A. Migdall, and S. V. Polyakov, Invited review article: Single-photon sources and detectors, *Rev. Sci. Instrum.* **82**, 071101 (2011).
- [48] Hongchao Xie, Shengwei Jiang, Jie Shan, and Kin Fai Mak, Valley-selective exciton bistability in a suspended monolayer semiconductor, *Nano Lett.* **18**, 3213 (2018).